

Optical Optimization of Passivated GaAs Nanowire Solar Cells

Kyle W. Robertson*, Ray R. LaPierre ‡, Jacob J. Krich*†

*Department of Physics, University of Ottawa, Ottawa, ON, K1N 6N5, Canada

†School of Electrical Engineering and Computer Science, University of Ottawa, Ottawa, Ontario, K1N 6N5, Canada

‡Department of Engineering Physics, McMaster University, Hamilton, Ontario, L8S 4L7, Canada

Abstract—We utilize rigorous coupled wave analysis (RCWA) to optimize the optical design of GaAs nanowire solar cells. RCWA is highly accurate while being less computationally expensive than competing techniques. Using a simplex optimization method, we determine the optimal device geometries that maximize photocurrent density for bare nanowires and contacted nanowires in a dielectric material with a top ITO contact, finding agreement with previous work. We extend these results to include passivating shells, which are required for efficient devices. These optimizations give important guidance for geometric design of nanowire solar cell devices.

I. INTRODUCTION

Nanowire solar cells (NWSC) have emerged as promising candidates for highly efficient, inexpensive solar energy harvesters offering many unique benefits. With the correct choice of nanowire array geometry, one can reduce material requirements relative to flat-panel solar cells without sacrificing absorption or device efficiencies.

Nanowire solar cells inherently require less active semiconductor material relative to planar solar cells, making them a potentially less expensive alternative to conventional solar cell designs. The small cross-sectional area of the nanowires allows them to be grown on lattice-mismatched substrates with the resulting strain accommodated without dislocations. This flexibility enables growth on inexpensive substrates and creation of tandem solar cells of lattice-mismatched materials, further reducing cost and improving potential efficiency [1], [2].

The excellent broadband absorption of NWSC has been widely demonstrated [3]–[6] and is due to nanowires having larger absorption cross sections than their physical cross sections. This increased absorption cross section results from a self-concentrating effect [7] that focuses carrier generation into the tip of the nanowire. The optical modes of the nanowire create internal resonances that enhance overall absorption [8]–[10]. The geometric design of the nanowire structure must be properly optimized to maximize the benefit of these performance-enhancing effects.

Despite the promising optical properties of NWSC, their large surface area contributes to high levels of surface recombination in GaAs nanowires. This problem has been solved by introducing a passivating shell of higher bandgap material

around the nanowire core (as illustrated in Figure 1), which has proven to be an effective method for increasing device performance [11]–[13].

While the necessity of a passivating shell for electrical device performance has been well demonstrated [14], little work has been done to investigate the optical consequences of adding such a shell. Because the shell material has a higher bandgap and different optical properties than the core material, it has the potential to change the optical characteristics of nanowire devices and thus the optimal geometric design. Huang and Povinelli consider AlGaAs passivation shells without planarizing dielectric and ITO contact [15]. In this work, we use rigorous coupled wave analysis (RCWA) to perform wave-optics simulations of a square array of cylindrical GaAs nanowires passivated by AlInP shells including conducting ITO and planarizing dielectric, which are important for real devices. We discuss the advantages of the RCWA method and present the shell thickness, core radius, and array periodicity that optimize the maximal photocurrent density J_{ph} . We then give valuable guidance for the design of optical NWSC arrays.

II. METHODS

RCWA (also referred to as the Fourier modal method) is a semi-analytic, frequency-domain method for solving Maxwell’s equations [16], [17]. Unlike the finite element method (FEM) or finite difference methods, RCWA propagates fields in the z -direction analytically, reducing the number of discretized dimensions from three to two. This analytic propagation requires the device to be composed of discrete layers, where the material parameters must be constant along the z -direction within a layer. Vertical nanowire designs (see Figure 1) are ideal systems for such analysis. Because the axial spatial direction is treated analytically, simulation times are independent of the layer thicknesses and any number of layer thicknesses can be explored during a single simulation essentially for free. We implement our model using the open-source RCWA library S^4 [18]. At each frequency, S^4 expands the electromagnetic fields within each layer using a 2D plane-wave basis with exponential dependence in the axial direction. The fields are made to satisfy continuity conditions at layer interfaces using the S-matrix algorithm [18].

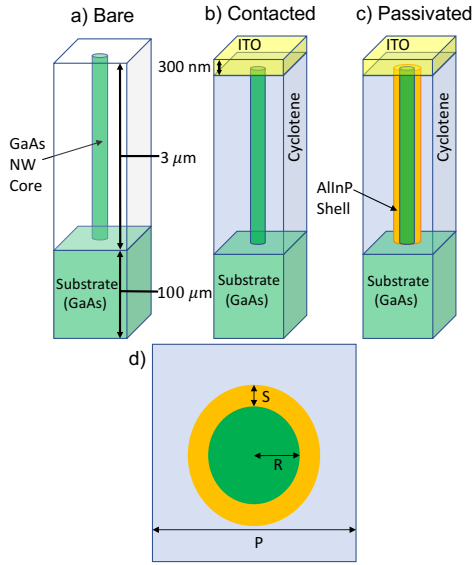


Fig. 1. A single unit cell of the square lattice nanowire array. a) An unpassivated and uncontacted bare nanowire. b) An unpassivated, contacted nanowire planarized with dielectric material. Although there is a non-trivial geometry in the x-y plane, the material parameters remain constant along z within each layer. c) A fully passivated nanowire. d) A top down view of the nanowire layer with core radius R , array period P , and shell thickness S .

We simulate nanowire array absorption by dividing the AM1.5G spectrum into 120 equally spaced frequency bins from 350-900 nm. A circularly polarized plane wave is injected at normal incidence onto the first layer of the device. Due to the circular symmetry of the nanowire, this polarization choice removes the need to simulate two independent polarizations for incoherent illumination [14]. We impose periodic boundary conditions at the x and y limits of the simulation domain to simulate an array of nanowires. The materials are defined through their frequency-dependent refractive index n and extinction coefficient k taken from bulk material [19], [20]. Referring to Fig. 1, we first model a bare nanowire. We then model a nanowire contacted by a top layer of ITO and planarized with a cyclotene dielectric (contacted nanowire). Finally, we model a contacted, planarized, passivated nanowire (passivated nanowire).

We seek to maximize the photocurrent density, where we assume that each absorbed photon produces one excited electron. Thus, we maximize spectral absorptance weighted by photon number

$$\bar{A} = \frac{\int_{\lambda_1}^{\lambda_2} \frac{\lambda}{hc} A(\lambda) I(\lambda) d\lambda}{\int_{\lambda_1}^{\lambda_2} \frac{\lambda}{hc} I(\lambda) d\lambda} \quad (1)$$

where λ is the photon wavelength, h is Planck's constant, c is the speed of light, $A(\lambda)$ is the wavelength dependent absorptance of the NWSC, $I(\lambda)$ is the AM1.5G spectrum in $\text{W}\cdot\text{m}^{-2}\cdot\text{nm}^{-1}$ [21], and hc/λ is the energy of the incident photon. The integration limits are $\lambda_1 = 350$ nm and $\lambda_2 = 900$ nm, which contains all photons with wavelength

shorter than the GaAs band gap of 870.5 nm. Assuming perfect carrier collection, the photocurrent density would be

$$J_{ph} = \frac{q}{hc} \int_{\lambda_1}^{\lambda_2} \lambda A(\lambda) I(\lambda) d\lambda \quad (2)$$

which is directly relatable to Eq. (1) by $J_{ph} = \bar{A} \cdot 33.37$ mA/cm². We obtain the wavelength-dependent absorption coefficients from

$$R(\lambda) = \frac{P_{ref}}{P_{in}} \quad (3)$$

$$T(\lambda) = \frac{P_{tran}}{P_{in}} \quad (4)$$

$$A(\lambda) = 1 - R(\lambda) - T(\lambda) \quad (5)$$

where P_{in} is the incident power, and P_{ref} and P_{tran} are the reflected and transmitted powers, respectively.

There exists a subtle but important detail concerning in which regions of the device we choose to calculate the absorptance A . Referring back to Figure 1, there are two reasonable choices. The first choice would be to consider A of the entire device, including the substrate. The second choice would be to instead consider A of only the nanowire, neglecting any absorption in the substrate. Computationally, this comes down to a choice of where we calculate $T(\lambda)$. The first choice places the calculation at the bottom of the substrate, while the second places the calculation at the nanowire-substrate interface.

Collection of carriers generated in the substrate is dependent on the diffusion length of the carrier, and thus also on the material quality of the substrate. Assuming reasonable diffusion lengths in the substrate, most carriers generated in the substrate are not collectable [14]. We therefore want to maximize the number of charge carriers generated in the nanowire near the p-n junction of the device. This choice decreases the distance carriers must travel to reach the junction and thus increases their likelihood of being separated and collected. In axial junction nanowires, the junction is usually placed near the top of the nanowire core. By choosing to optimize A of only the nanowire and ignoring any absorption in the substrate, the optimizer searches for a device geometry that shifts absorption into the nanowire. This geometric optimization achieves the desired effect of concentrating carrier generation near the junction. In this work we choose to calculate $T(\lambda)$ at the nanowire-substrate interface and thus all absorptance values exclude absorption in the substrate. Note these absorptance values include the absorptance of the ITO layer. For the optimized contacted nanowire, ITO absorption only contributes 2.6% to the integrated absorptance and does not significantly affect the resulting optimal geometric parameters.

As a first example of modeling NWSC via the RCWA method, we use Nelder-Mead simplex optimization to find the optimal array period and nanowire radius. This optimization allows us to find the desired geometric parameters to high precision without the unnecessary overhead of blind parameter sweeps. During all optimizations, the ITO thickness is fixed at 300 nm, the nanowire length at 3 μm , and the substrate thickness at 100 μm .

TABLE I

Optimizations results for bare and contacted nanowires. J_{ph} includes absorption in the ITO and nanowire layers and excludes the substrate.

System	Array Period [nm]	Core Radius [nm]	J_{ph} [mA cm ⁻²]
Bare Nanowire	338	85	29.37
Contacted nanowire	326	103	28.55

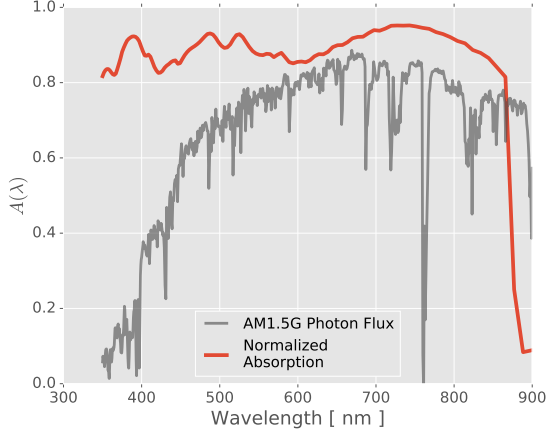


Fig. 2. Absorbance, $A(\lambda)$, in the ITO and nanowire regions of the optimized contacted nanowire (see Table I) plotted with the photon-weighted AM1.5G spectrum, $\frac{\lambda}{hc}I(\lambda)$, in arbitrary units.

We find the array period and core radius that maximize J_{ph} for the bare nanowire (shown in Table I), in good agreement with previous FEM-based results [19]. We use results from this optimization as a starting point to find the optimal parameters for the contacted nanowire. We go on to extend previous work by exploring the effects of adding an AlInP passivating shell of varying thickness to the contacted nanowire and optimizing the array period and core radius for passivated nanowire structures.

III. RESULTS

A. Bare & Contacted Nanowire

When ITO and cyclotene are added to the optimized bare nanowire, J_{ph} drops from 29.37 mA/cm² to 28.01 mA/cm². Reoptimizing the geometry recovers 40% of the loss to J_{ph} , resulting in a value of 28.55 mA/cm². Table I shows the optimal geometric parameters for the bare nanowire and the contacted nanowire, indicating the small change in the optimal array period and 21% change in the optimal core radius when the ITO and dielectric are included. The absorption spectrum of the ITO and nanowire layers for a contacted nanowire using those parameters is shown in Figure 2. As expected, the geometry of the nanowire is tuned to place an absorption peak near the strongest part of the spectrum, between roughly 600-800 nm. Figure 3 shows the generation rate $G(\vec{r})$ along a 2D slice through the contacted nanowire [14],

$$G(\vec{r}) = \sum_i \frac{\epsilon_0}{\hbar} |E(\lambda_i, \vec{r})|^2 n(\lambda_i) k(\lambda_i) \quad (6)$$

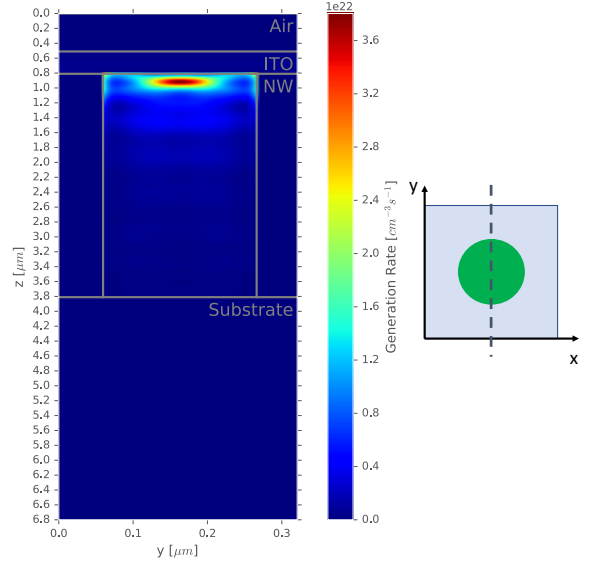


Fig. 3. Generation rate in a contacted nanowire along a fixed y - z plane through the center of the nanowire core, as shown in the schematic on the right. The nanowire is stretched horizontally for clarity. Strong self-concentrating of light at the tip of the nanowire is apparent.

where λ_i are the simulated wavelengths, $E(\lambda_i, \vec{r})$ is the electric field at wavelength λ_i and position vector \vec{r} , ϵ_0 is the vacuum permittivity, and \hbar is the reduced Planck's constant. Our optimization has concentrated carrier generation within the desired region at the tip of the nanowire.

B. Passivated Nanowire

Optically, there is no benefit to including a passivating shell. Instead, we look for the best optical designs including the electrically-necessary passivation. First, we sweep through shell thicknesses of 10-80 nm while keeping the total core+shell radius fixed at 103 nm and array period fixed at 326 nm, which are the optimal values for the contacted nanowire (see Table I). Results in Figure 4 show that, for shells thinner than 40 nm, absorption losses are minimal and that dramatic losses occur when including a thicker shell. In terms of overall performance, the passivating shell is a necessity and the small absorption gains accrued from removing it do not outweigh the performance costs due to surface recombination.

Reoptimizing to find the optimal core radius and array period at each shell thickness recovers almost entirely the optical properties of the contacted nanowire (see Figure 4). Here lies the value of device optimization through simulation. We see that by reoptimizing the geometry of the nanowire array, losses to J_{ph} can be almost entirely recovered and it is possible to achieve the electrical benefits of a passivating shell without negatively affecting device absorption.

The parameter values resulting from our optimization are shown in Figure 5. These parameters vary considerably from the contacted nanowire optimal values, and in general one needs to increase the array period and decrease the core radius as the shell thickness increases. A large change in optimal geometric parameters occurs at a 40 nm shell thickness. At a

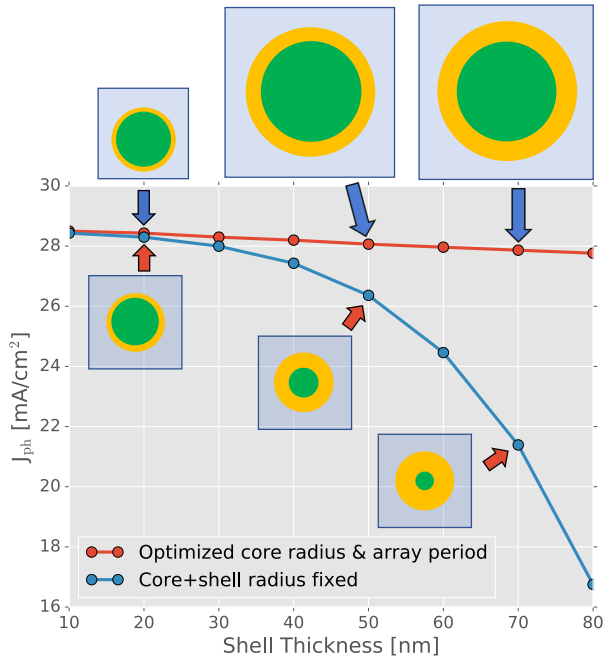


Fig. 4. Maximal photocurrent densities for passivated nanowires with fixed shell thickness. The unoptimized data has an array period of 326 nm and the sum of the core radius and shell thickness fixed to 103 nm (see Table I). The optimized data are the maximal photocurrent densities resulting from a reoptimization of the array period and core radius at each shell thickness. Insets are to-scale representations of the top-down view of the nanowire geometries.

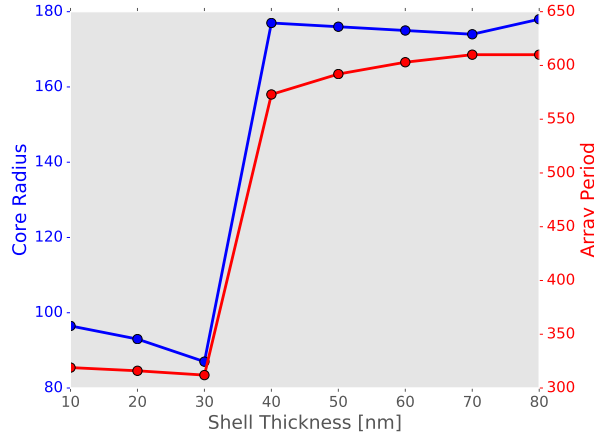


Fig. 5. Reoptimized core radius (left axis) and array period (right axis) that give the maximum possible J_{ph} for fixed shell thicknesses in the passivated nanowires, corresponding to Figure 4. Lines are guides to the eye.

40 nm shell thickness, two local optima exist in the parameter space, which differ in J_{ph} by only 0.004% (see Figure 6). Below a 40 nm shell thickness, the small-period optimum is the global optimum. At and above a 40 nm shell thickness, the large-period optimum is the global optimum. For a shell thickness of 70 nm, the two optima differ by 1.2%.

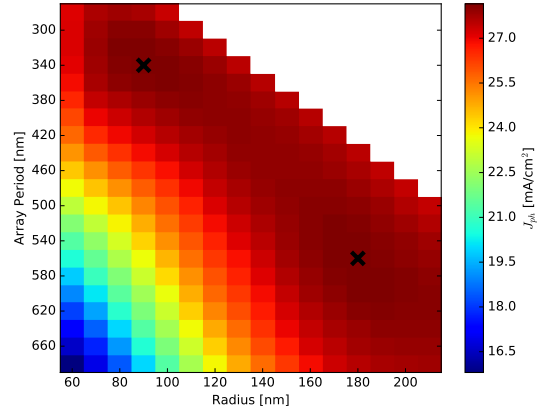


Fig. 6. A heatmap showing the photocurrent density for a shell thickness of 40 nm as a function of the array period and core radius. The white regions correspond to a combined core+shell diameter that would have exceeded the array period at that point. The two local optima are marked with a small x.

IV. CONCLUSION

In this paper, we describe a method for efficient optical simulation of NWSC devices. Our first demonstration of this method is a geometric optimization to maximize photon-weighted optical absorption. This method will be useful for combined optical and electrical simulations [14], with a significant reduction in computational cost. We find that optimal absorption occurs in the absence of a passivating shell, and outline the losses to the photocurrent density as a function of the shell thickness. In the presence of a shell of fixed thickness, we present the array period and core radius that maximize the photocurrent density and show that by reoptimizing the nanowire geometry the losses incurred by adding a shell can be almost completely recovered. This information will be invaluable for use in growing efficient GaAs NWSC.

REFERENCES

- [1] K. L. Kavanagh, "Misfit dislocations in nanowire heterostructures," *Semiconductor Science and Technology*, vol. 25, no. 2, p. 024006, 2010.
- [2] V. Dhaka, T. Haggren, H. Jussila, H. Jiang, E. Kauppinen, T. Huhtio, M. Sopenan, and H. Lipsanen, "High Quality GaAs Nanowires Grown on Glass Substrates," *Nano Letters*, vol. 12, no. 4, pp. 1912–1918, Apr. 2012.
- [3] L. Hu and G. Chen, "Analysis of Optical Absorption in Silicon Nanowire Arrays for Photovoltaic Applications," *Nano Letters*, vol. 7, no. 11, pp. 3249–3252, Nov. 2007.
- [4] J. Zhu, Z. Yu, G. F. Burkhard, C.-M. Hsu, S. T. Connor, Y. Xu, Q. Wang, M. McGehee, S. Fan, and Y. Cui, "Optical Absorption Enhancement in Amorphous Silicon Nanowire and Nanocone Arrays," *Nano Letters*, vol. 9, no. 1, pp. 279–282, Jan. 2009.
- [5] M. D. Kelzenberg, S. W. Boettcher, J. A. Petykiewicz, D. B. Turner-Evans, M. C. Putnam, E. L. Warren, J. M. Spurgeon, R. M. Briggs, N. S. Lewis, and H. A. Atwater, "Enhanced absorption and carrier collection in Si wire arrays for photovoltaic applications," *Nature Materials*, vol. 9, no. 3, pp. 239–244, Mar. 2010.
- [6] M. Yao, N. Huang, S. Cong, C.-Y. Chi, M. A. Seyedi, Y.-T. Lin, Y. Cao, M. L. Povinelli, P. D. Dapkus, and C. Zhou, "GaAs Nanowire Array Solar Cells with Axial pin Junctions," *Nano Letters*, vol. 14, no. 6, pp. 3293–3303, Jun. 2014.
- [7] X. Wang, M. R. Khan, M. Lundstrom, and P. Bermel, "Performance-limiting factors for GaAs-based single nanowire photovoltaics," *Optics Express*, vol. 22, no. S2, p. A344, Mar. 2014.

- [8] L. Cao, P. Fan, A. P. Vasudev, J. S. White, Z. Yu, W. Cai, J. A. Schuller, S. Fan, and M. L. Brongersma, "Semiconductor Nanowire Optical Antenna Solar Absorbers," *Nano Letters*, vol. 10, no. 2, pp. 439–445, Feb. 2010.
- [9] D. Wu, X. Tang, K. Wang, and X. Li, "An Analytic Approach for Optimal Geometrical Design of GaAs Nanowires for Maximal Light Harvesting in Photovoltaic Cells," *Scientific Reports*, vol. 7, 2017.
- [10] K. T. Fountaine, W. S. Whitney, and H. A. Atwater, "Resonant absorption in semiconductor nanowires and nanowire arrays: Relating leaky waveguide modes to Bloch photonic crystal modes," *Journal of Applied Physics*, vol. 116, no. 15, p. 153106, Oct. 2014.
- [11] R. R. LaPierre, "Numerical model of current-voltage characteristics and efficiency of GaAs nanowire solar cells," *Journal of Applied Physics*, vol. 109, no. 3, p. 034311, Feb. 2011.
- [12] I. Åberg, G. Vescovi, D. Asoli, U. Naseem, J. P. Gilboy, C. Sundvall, A. Dahlgren, K. E. Svensson, N. Anttu, M. T. Björk, and L. Samuelson, "A GaAs Nanowire Array Solar Cell With 15.3% Efficiency at 1 Sun," *IEEE Journal of Photovoltaics*, vol. 6, no. 1, pp. 185–190, Jan. 2016.
- [13] C.-C. Chang, C.-Y. Chi, M. Yao, N. Huang, C.-C. Chen, J. Theiss, A. W. Bushmaker, S. LaLumondiere, T.-W. Yeh, M. L. Povinelli, C. Zhou, P. D. Dapkus, and S. B. Cronin, "Electrical and Optical Characterization of Surface Passivation in GaAs Nanowires," *Nano Letters*, vol. 12, no. 9, pp. 4484–4489, Sep. 2012.
- [14] A. H. Trojnar, C. E. Valdivia, R. R. LaPierre, K. Hinzer, and J. J. Krich, "Optimizations of GaAs Nanowire Solar Cells," *IEEE Journal of Photovoltaics*, vol. 6, no. 6, pp. 1494–1501, Nov. 2016.
- [15] N. Huang and M. L. Povinelli, "Design of Passivation Layers on Axial Junction GaAs Nanowire Solar Cells," *IEEE Journal of Photovoltaics*, vol. 4, no. 6, pp. 1511–1517, Nov. 2014.
- [16] M. G. Moharam and T. K. Gaylord, "Rigorous coupled-wave analysis of planar-grating diffraction," *JOSA*, vol. 71, no. 7, pp. 811–818, Jul. 1981.
- [17] M. G. Moharam, T. K. Gaylord, E. B. Grann, and D. A. Pommet, "Formulation for stable and efficient implementation of the rigorous coupled-wave analysis of binary gratings," *JOSA a*, vol. 12, no. 5, pp. 1068–1076, 1995.
- [18] V. Liu and S. Fan, "S4 : A free electromagnetic solver for layered periodic structures," *Computer Physics Communications*, vol. 183, no. 10, pp. 2233–2244, Oct. 2012.
- [19] Y. Hu, R. R. LaPierre, M. Li, K. Chen, and J.-J. He, "Optical characteristics of GaAs nanowire solar cells," *Journal of Applied Physics*, vol. 112, no. 10, p. 104311, 2012.
- [20] S. Adachi, *Optical Constants of Crystalline and Amorphous Semiconductors: Numerical Data and Graphical Information*. New York: Springer Science + Business Media, LLC, 1999.
- [21] "Standard Tables for Reference Solar Spectral Irradiances: Direct Normal and Hemispherical on 37 Tilted Surface," ASTM International, Tech. Rep., 2012.